Numerical study of the propagation of ionization processes in an oxygen Z-pinch plasma

Seong Ho Kim, Ki-Tae Lee, Dong-Eon Kim, and Tong Nyong Lee
Department of Physics, Pohang University of Science and Technology, San 31 Hyoja-Dong, Pohang, Kyungbuk 790-784, Korea

(Received 25 July 1996; accepted 11 December 1996)

The dynamics of the ionization processes in an oxygen Z-pinch plasma has been numerically studied. Ionization balance equations incorporated in single-fluid magnetohydrodynamics (MHD) equations were solved. The focus was on the imploding phase before a shock wave was fully developed. It was shown that the propagation speed of an ionization stage is larger than the fluid speed. For example, the propagation speed of O III ionization stage is faster than the fluid speed at the position of the peak density of O III particles. The larger propagation speeds of ionization stages than the fluid speed result from the propagation of Joule heating power. © *1997 American Institute of Physics.* [S1070-664X(97)02703-1]

I. INTRODUCTION

Z-pinch is the implosion of a plasma column due to self-magnetic pressure generated by an axial current. A plasma produced in a pulsed Z-pinch device easily reaches high temperature and high density. Such a plasma is useful for the spectroscopic study of highly ionized atoms.[1] Among the devices producing a Z-pinch plasma such as vacuum spark, plasma focus, and gas-puff Z-pinch devices, the gas-puff Z-pinch is considered to produce the most efficient and intense pulsed x-rays.[2] It is operated by injecting a gas shell between two electrodes inside a vacuum chamber and initiating a high voltage discharge at a proper time. Copious soft and hard x-rays are emitted when the cylindrical plasma is pinched. The pinching time can be adjusted by varying initial gas-load mass and geometry, which is one of the essential advantages over the other devices mentioned above. The device may be also used as a soft x-ray source for x-ray microscopy and x-ray lithography.[3]

Much research in the past has been concentrated on the study of x-ray production from the gas-puff Z-pinch for applications to x-ray microscopy, lithography, etc. Mainly, the K- and M-shell radiations from the gas-puff Z-pinch plasma have been theoretically and experimentally investigated around the pinch time.[4–6] On the other hand, little attention has been paid to the dynamical behavior in an imploding phase; only the radial implosion profiles have been measured and compared with the simple model such as snowplow.[7,8] Even though the importance of the initial implosion phase where the gas is ionized and accelerated to the axis has been pointed out,[9] the behavior of the ionization stages in the implosion phase has not been much studied.

Foord *et al.* have recently measured the time- and space-resolved spectra of the several ultraviolet (UV) lines from oxygen ions produced in a CO_2 plasma.[10] They showed that O II ionization stage propagates faster than O II particles. They proposed an ionization wave whose front ionizes the neutral gases before it. They suggested that by a simple balance between thermal heat flux and ionization energy, the electron heat conduction from the rear region (large radius) of the shell would be a possible driving force for the fast motion of an O II ionization stage. Since the distribution of the magnetic field or current densities inside the shell could not be measured, the role of the magnetic field was not properly discussed. They observed that the low ionization stages exist in the front region (small radius) of the plasma shell and the high ionization stages in the rear region, which is inconsistent with an existing theory by Barak and Rostoker. Their model predicts that highly-charged ions would exist in the front region of a moving plasma shell.[11]

Motivated by Foord's study, we have carried out a numerical simulation on an oxygen Z-pinch plasma. We have focused our attention on the behavior of O III and higher ionization stages and the role of the magnetic field. In this paper, the detailed dynamical study of the ionization stages is presented under conditions similar to Foord's experiment and the role of the relevant driving forces, such as Joule heating due to the diffusion of magnetic field, thermal conduction, and shock heating, is also discussed. The computer code used in this study solves one-dimensional magnetohydrodynamics (MHD) equations coupled with ionization balance equations, which are briefly discussed in the following section.[12]

II. MAGNETOHYDRODYNAMIC MODELING

The MHD model adopted in the present study consists of one-dimensional MHD equations of single-fluid with two-temperature and ionization balance equations for the evaluation of the population density of the ground state in each ionization stage of oxygen. The heat conduction, Joule heating, and bremsstrahlung radiation are taken into account and the effects of ionization, recombination, and resonance line radiation are also included. The equations in the cylindrical geometry are as follows.

The continuity equation is

$$\frac{dN_i}{dt}+\frac{N_i}{r}\frac{\partial(rv)}{\partial r}=0, \tag{1}$$

where $d/dt=\partial/\partial t+v(\partial/\partial r)$, N_i the ion density, and v the fluid velocity in the radial direction.

The momentum equation is

 1070-664X/97/4(3)/730/7/$10.00

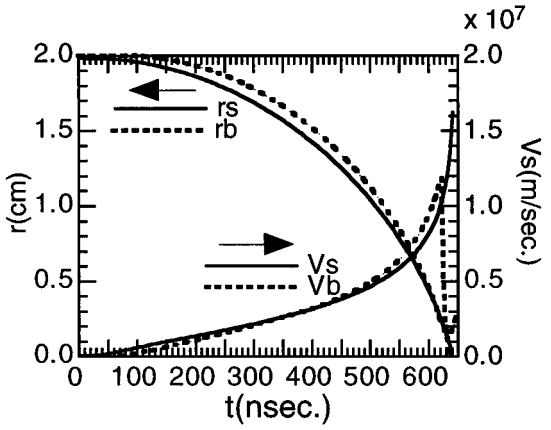

FIG. 1. The motion of plasma boundary. The MHD simulation is compared with the result from snowplow model. r_s, v_s are radial position and velocity by snowplow model and r_b, v_b are radial position and velocity of plasma boundary by numerical simulation.

$$m_i N_i \frac{dv}{dt} = -\frac{\partial}{\partial r}(N_e T_e + N_i T_i) - \frac{B}{4\pi r}\frac{\partial (rB)}{\partial r} - 2\frac{v}{r}\frac{\partial \chi}{\partial r} + \frac{\partial}{\partial r}\left(\frac{4}{3}\frac{\chi}{r}\frac{\partial (rv)}{\partial r}\right), \tag{2}$$

where m_i is the ion mass, N_e the electron density, T_e, T_i the electron and ion temperature, respectively. B is the azimuthal component of the magnetic field induced by the axial current and χ is the artificial shock viscosity given by

$$\chi = \begin{cases} \frac{1}{2} c_q l^2 m_i N_i \frac{1}{r}\left|\frac{\partial}{\partial r}(rv)\right| & \left(\frac{\partial v}{\partial r}\right) < 0, \\ 0 & \left(\frac{\partial v}{\partial r}\right) > 0, \end{cases} \quad (\mathrm{g\ cm^{-1}\ s^{-1}}), \tag{3}$$

where c_q is a constant to control the shock region. The artificial shock viscosity plays a role of smoothing plasma parameters near a shock region without violating physics[9,13] and provides the shock wave with a dissipative mechanism as shown below in Eq. (5).

The temperature evolution equation for the electron is

$$\frac{dT_e}{dt} = -\frac{2}{3} T_e \frac{1}{r}\frac{\partial (rv)}{\partial r} + \frac{2}{3}\frac{1}{N_e r}\frac{\partial}{\partial r}\left(\kappa_{e\perp} r \frac{\partial T_e}{\partial r}\right) + \frac{2}{3}\frac{1}{N_e}(P_J - P_{\mathrm{brem}} - P_{\mathrm{atom}}) - P_{ei}, \tag{4}$$

where $\kappa_{e\perp}$ is the electron heat conductivity,[14] P_J the Joule heating and P_{brem} the bremsstrahlung radiation loss. P_{Atom} is

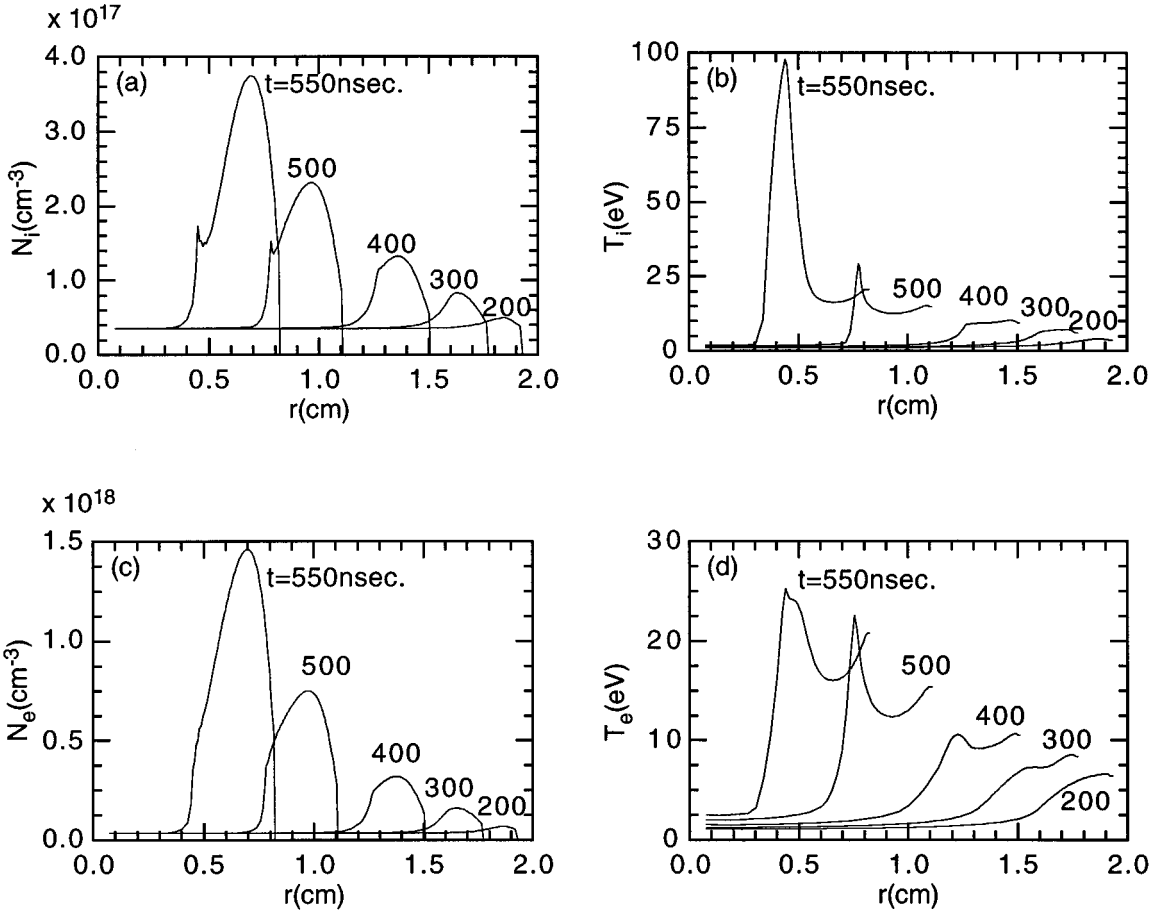

FIG. 2. The evolution of the spatial distribution of (a) ion density, (b) ion temperature, (c) electron density, and (d) electron temperature.

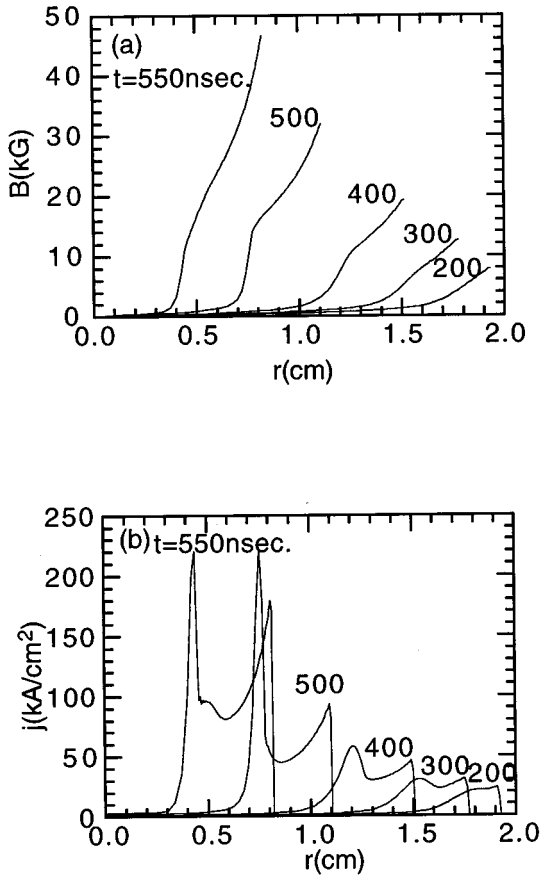

FIG. 3. The spatial distribution of (a) magnetic field and (b) current density at various times.

the loss due to atomic processes, which include energy loss by collisional ionization and resonance line radiation and heating by recombination. P_{ei} is the energy equilibration between the electron and the ion.

The temperature evolution equation for an ion is

$$\frac{dT_i}{dt} = -\frac{2}{3}T_i\frac{1}{r}\frac{\partial(rv)}{\partial r} + \frac{2}{3}\frac{1}{N_i}\frac{\partial}{\partial r}\left(\kappa_{i\perp} r\frac{\partial T_i}{\partial r}\right) + \frac{2}{3}\frac{\chi}{N_i}\left[\frac{1}{3}\left(\frac{1}{r}\frac{\partial(rv)}{\partial r}\right)^2 + \left(r\frac{\partial}{\partial r}\left(\frac{v}{r}\right)\right)^2\right] + P_{ei}, \quad (5)$$

where $\kappa_{i\perp}$ is the ion heat conductivity.

The magnetic field transport equation is

$$\frac{dB}{dt} = -B\frac{\partial v}{\partial r} + \frac{\partial}{\partial r}\left(\frac{c^2}{4\pi}\frac{\eta_\perp}{r}\frac{\partial(rB)}{\partial r}\right), \quad (6)$$

where $\eta_\perp$ is the plasma resistivity.

Ionization balance equations calculating the fractional ground-state population are

$$\frac{dn_z}{dt} = -N_e n_z\alpha_z - N_e n_z R_z + N_e n_{z+1}\alpha_{z+1} + N_e n_{z-1}R_{z-1}, \quad (7)$$

where n_z is the fractional ground-state population of the ionization stage of charge z to the total ion density N_i and $\Sigma_z n_z = 1$. α_z and R_z are the recombination and ionization rate coefficient, respectively.

The single-fluid model implicitly assumes that the ions of different ionization stages move together and share the same temperature. This assumption is justified if collisional processes between different ions are very fast so that the slowing-down time and the energy equilibration time between different ions[15] are very small compared to the characteristic time-scale of the change of other macroscopic plasma parameters such as density and temperature. Under the simulation conditions of the present study, the slowing-down and the energy equilibration time have been computed to be about three orders of magnitude smaller than the time-scale of the change of density and temperature. In general, the collisional processes between ions are very fast so that the single-fluid model has been widely used. Fisser and Schlüter have shown that the magnetic field distribution calculated by the single-fluid model is in good agreement with the experimental observation in a Z-pinch similar to ours.[16]

The equations are solved in the Lagrangian scheme, and the detailed numerical methods were discussed in Ref. 12.

The boundary conditions are

$$\left.\frac{\partial T_e}{\partial r}\right|_{r=0} = \left.\frac{\partial T_i}{\partial r}\right|_{r=0} = 0, \quad (8)$$

$$B(r=0)=0, \quad v(r=0)=0, \quad (9)$$

$$\left.\frac{\partial T_e}{\partial r}\right|_{r=r_p} = \left.\frac{\partial T_i}{\partial r}\right|_{r=r_p} = 0, \quad (10)$$

$$\left[\frac{4}{3}\chi\left(\frac{\partial v}{\partial r} - \frac{1}{2}\frac{v}{r}\right) - (N_e T_e + N_i T_i)\right]_{r=r_p} = 0. \quad (11)$$

The boundary conditions reflect an axial symmetry at axis and represent that particles can not move through the plasma–vacuum interface. The vacuum density is specified as 3.5×10^8 cm^{-3}. A driving current, $I(t)$, simplified as a sinusoidal wave with peak current, I_0, and angular frequency, ω, is given by

$$I(t) = I_0 \sin(\omega t). \quad (12)$$

The azimuthal component of the magnetic field at the outer boundary of the plasma is then described by

$$B(r=r_p) = \frac{2I(t)}{r_p c}. \quad (13)$$

III. RESULTS

For the simulation, the peak value of a driving current was taken to be 290 kA with the quarter-period of 1.2 μs, which were the parameters in Foord's experiments.[10] The singly-ionized oxygen of $N_e = N_i = 3.5\times10^{16}$ cm^{-3} was initially taken to be uniformly distributed.

A. Dynamical properties

While the snowplow model predicts the pinch time and snowplow velocity reasonably well,[8,17] it does not yield de-

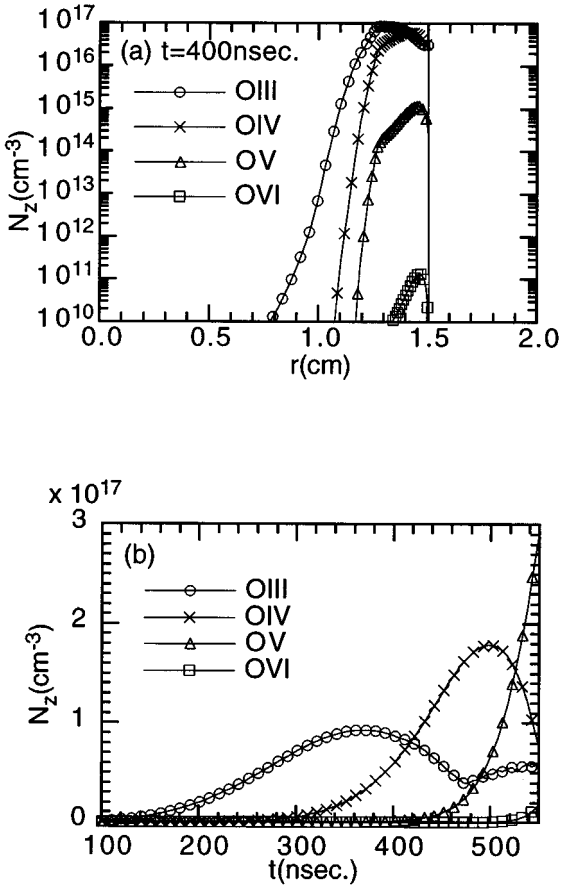

FIG. 4. Distributions of the ion densities of various ionization stages. (a) Spatial distributions of O III, O IV, and O V ionization stages at time $t=400$ ns, and (b) temporal evolutions of the peak densities of the O III to the O VI ionization stages.

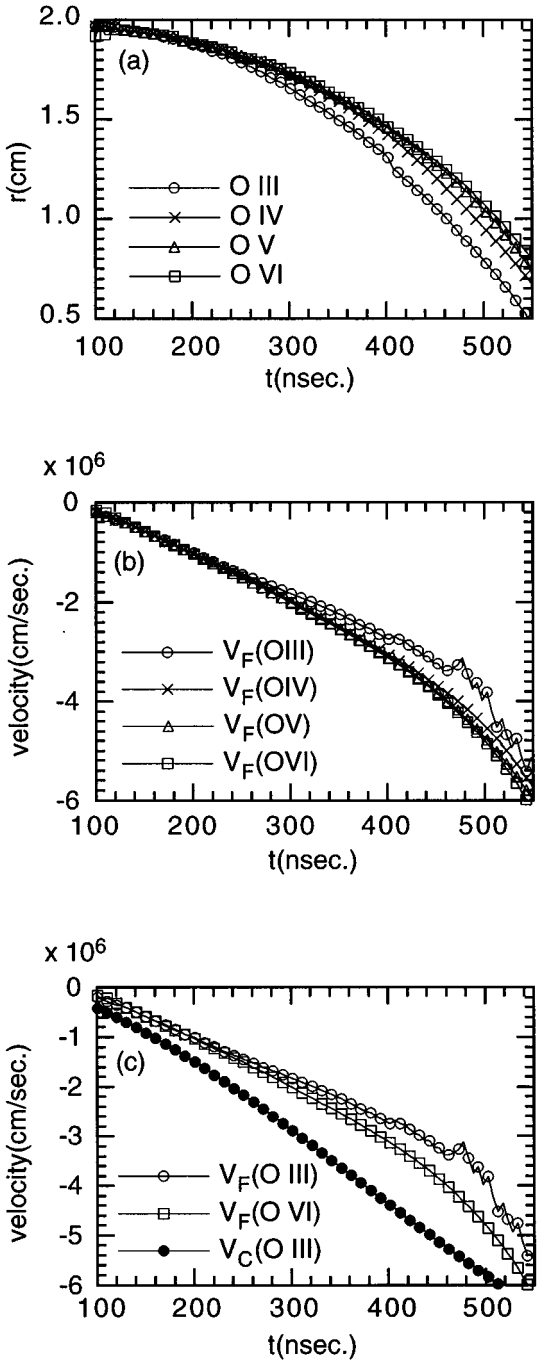

FIG. 5. The motions of ionization stages. (a) Positions of the peak densities of the ionization stages with respect to time, (b) fluid speed of a Lagrangian cell corresponding to the peak density of each ionization stage, and (c) the propagation speed (●) of O III ionization stage compared with the fluid speeds at the positions where the densities of the O III and O VI ionization stages are maximum.

tailed information about the plasma dynamics. The MHD model should be used to obtain more information about the fluid dynamics of plasma. The initially ionized plasma is accelerated toward the axis by magnetic pressure outside the plasma. As the current rises it is heated and ionized to higher ionization stages by heat conduction, Joule, and shock heating. When it reaches the axis, its kinetic energy is rapidly thermalized to produce a hot dense plasma column which subsequently experiences instabilities.

Figure 1 compares the motion of the plasma boundary obtained from computer simulation with that from the snowplow model. The plasma has pinched at 633 ns, which is in reasonable agreement with the observation,[10] resulting in the minimum radius of 1.5 mm, $N_e=6.4\times10^{19}$ cm^{-3}, $T_e=435$ eV, $N_i=9.6\times10^{18}$ cm^{-3}, and $T_i=1725$ eV. The snowplow model predicts that the radius of the plasma vanishes at the time of 641 ns, and the time to reach the radius of 1.5 mm is the same as that of our simulation.

The evolution of density and temperature distributions for an ion and an electron is shown in Fig. 2. As an implosion proceeds, the uniform density profile transforms into a shell-type profile by the time at $t=300$ ns. The profile has a width of about 2–3 mm, one-tenth of the initial diameter, and becomes more pronounced. The steep density profile drastically increases the shock heating power. This is manifested in the ion temperature profile where the temperature steeply rises from $t=500$ to 550 ns. The initial increase of the ion temperature is due to the energy-equilibration with the electron, but later in time the ion temperature steeply increases at the front due to the shock heating. The diffusion of the magnetic field due to the finite resistivity of the plasma is shown in Fig. 3(a). As the magnetic field diffuses into the interior region, the current density increases, as does the

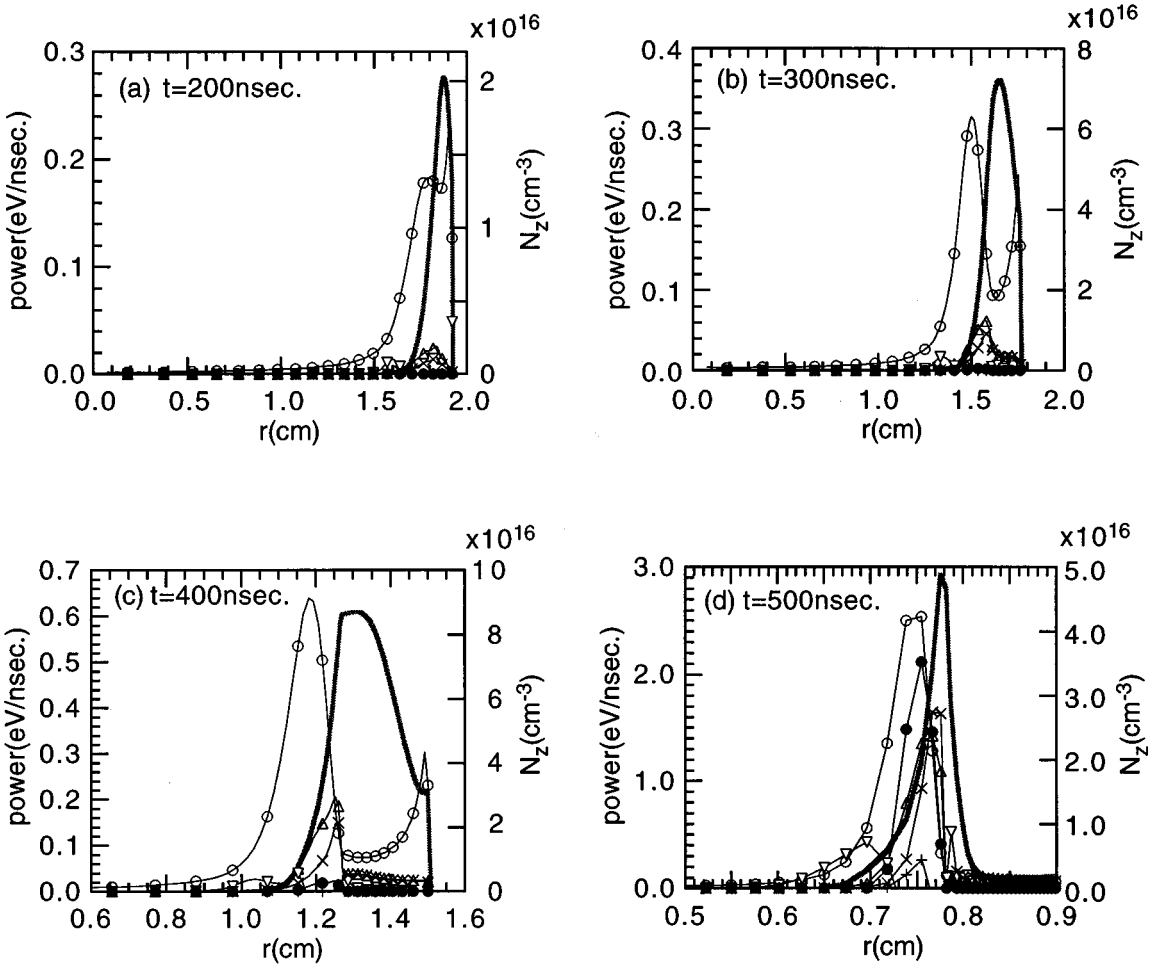

FIG. 6. Distribution of various power terms in the energy balance equations in comparison with the O III density profile (solid line) for different times: (a) 200 ns, (b) 300 ns, (c) 400 ns, and (d) 500 ns. P_J is the Joule heating (○), P_{ee},P_{ce} the adiabatic (△) and conduction heating (▽) by electrons, P_{ei},P_{ci} the adiabatic (×) and conduction heating (+) by ions, P_s the shock heating (●) by ions.

Joule heating. Thus it can be seen that the profile of the electron temperature follows that of the current density [Figs. 2(d) and 3(b)].

In Fig. 3(b) note that the current density profile has two peaks at both sides of the shock. The outer peak near the rear edge of the plasma is formed by the result of the snowplow and the shock at the front region originates from the shock wave front where the magnetic field penetration is hindered.[9]

B. Distribution and motion of ionization stages

The present study is focused on the dynamics of the ionization processes of ions and main driving powers for them.

Figure 4(a) shows the density distributions of various ionization stages. The low ionization stages are dominant in the front region of the moving plasma shell. The high ionization stages appear at the rear region, which agrees with the experimental observations.[10] This is due to the high electron temperature resulting from the large power deposited by Joule heating in the rear region. The temporal evolution of the peak densities of various ionization stages is presented in the Fig. 4(b). The O III ionization stage is dominant before the shell-type profile becomes clear about $t=500$ ns (Fig. 2). The density of the O III ionization stage reaches its peak at $t=370$ ns, at which the electron temperature is about 10 eV, about a third of the ionization potential of O III, 35 eV. As the shock develops, O IV, O V, and O VI ionization stages are rapidly generated. The steep density profiles are formed because of the localization by snowplow.

Figure 5(a) shows the positions of the peak densities of O III, O IV, O V, and O VI ionization stages with respect to time. Notice that the lower the ionization stage, the faster it moves ahead. Figure 5(b) shows the fluid velocities at the positions of the peak densities of various ionization stages. The fluid at the positions of the peak densities of high ionization stages, e.g., O V and O VI, which mostly exist in the rear region, moves faster than that of low ionization stages (O III, O IV). It can be explained by the fact that the acceleration by the $\mathbf{j}\times\mathbf{B}$ force is smaller in the front region than in the rear. In Figure 5(c) the propagation speed of the O III ionization stage is shown with the fluid velocity at the positions of the peak densities of O III and O VI ions. The propagation speed has been derived by the time-derivative of a fitting formula to the positions of the peak density of the O III ionization stage. The propagation of the O III ionization stage is faster than the motion of the fluid by a factor of

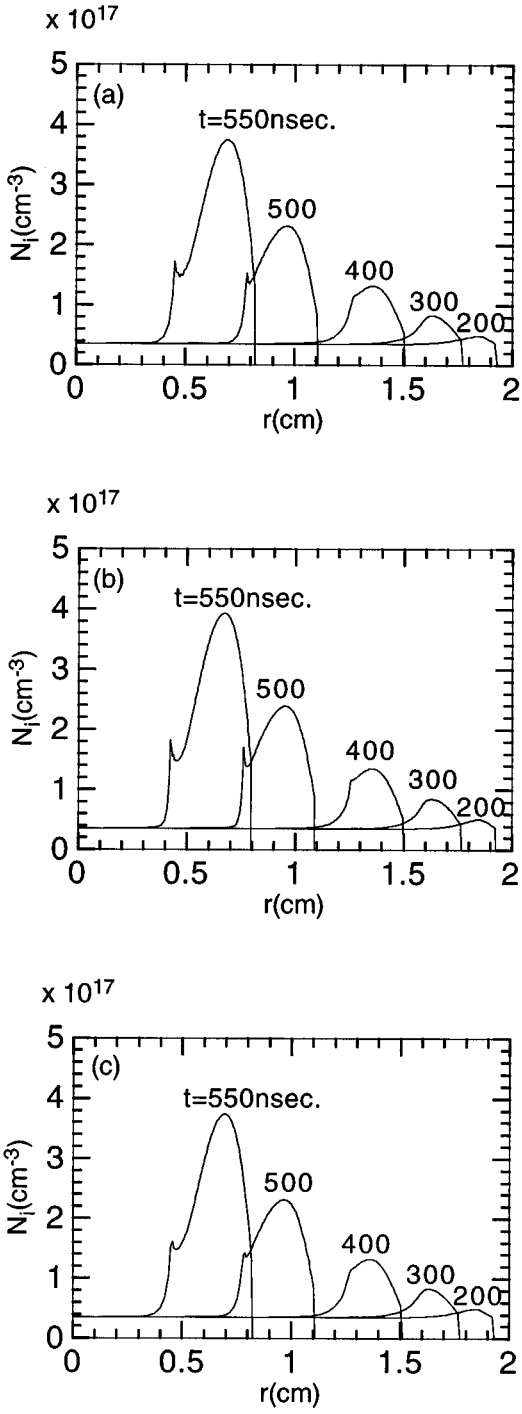

FIG. 7. Spatial profiles of the ion densities at various times for different values of c_q and the mesh number (n_x). (a) $c_q=3$, $n_x=100$; (b) $c_q=3$, $n_x=200$; (c) $c_q=5$, $n_x=100$.

1.5. When we fit all the curves of Fig. 5(a) using polynomials up to the 4th order and take the propagation speeds by the time-derivatives, the propagation speed is the highest for the O III ionization stage and decreases as the ionization number increases. However, each propagation speed is still higher than the fluid speed at the position of the peak density of each ionization stage.

Recent experimental observation by Foord *et al.* shows a similar result, in which the O II ionization stage propagates faster than any other ions.[10] By an estimation using a simple balance equation between thermal heat flux and ionization energy they claimed that the electron heat conduction from the outer region of the plasma would be responsible for the fast motion of the O II ionization stage. In our case, however, the propagation of an ionization stage is likely to be driven by Joule heat flux. We have plotted the spatial distribution of various heating power terms with the profile of the O III ionization stage at various times in Fig. 6: Joule heating, adiabatic, and conduction heating by electron and ions, and ion shock heating. Other power-terms related with bremsstrahlung, resonance line radiation, and electron–ion energy exchange were negligible in the imploding phase. As shown in Fig. 6, Joule heating power is higher than any other power term and leads the O III ionization stage in the imploding phase. This result suggests that the Joule heating power propagates earlier than the other terms and ionizes the O II ions into O III. When the shock structure develops, e.g., at 550 ns, the shock heating power increases steeply and the abrupt increase of plasma temperature reduces the plasma resistivity, which leads to the drastic decrease of Joule heating power. As the shock is fully developed, the adiabatic compression, heat conduction, and shock heating play more important roles in the variation of density and temperature.[12] This result indicates that the main power to ionize the ion species is the Joule heating in the imploding phase, and the fact that the Joule heating leads the profile of O III indicates that the energy transport takes place as fast as the propagation of the O III ionization stage.

The artificial viscosity used in Eqs. (2) and (5) has been widely used to properly describe a region where there exists a steep gradient of physical parameters. In our simulation presented in the above, $c_q=3$ was used with the number of meshes being 100. Several simulations with the same physical parameters have been done under different values of c_q and the mesh number. The result is shown in Fig. 7 for the time-variations of the ion temperature profiles. Note that the difference between the different conditions is very small. It is also true for other physical parameters. This indicates that the results presented in the above is insensitive to the technical conditions of simulation and supports that the results are physical.

IV. CONCLUSION

We have numerically studied the dynamics of an oxygen Z-pinch plasma in the imploding phase under the conditions of the driving current and the quarter-period being 290 kA and 1.2 μs, respectively. The result shows that a plasma shell is formed at $t=300$ ns which is about half the pinch time. Until $t=500$ ns, the plasma is heated and ionized by Joule heating power. In this imploding phase the different ionization stages move with slightly different velocities. The low ionization stages exist in the front region, while the high ionization stages are produced in the rear region because of a high ionization rate via the overall effect of temperature, density, and Joule heating. The fluid at the region where low ionization stages are dominant moves more slowly in the shell than at the region where high ionization stages are dominant. However, for the propagation speed of each ion-

ization stage, the lower the ionization stage, the faster it moves. From examining the distribution of heating powers, it is shown that Joule heating is the most responsible source for the fast ionization of ion species compared with other heating sources in the imploding phase.

Though we have not included the existence of neutral gas, the motion of ion species showed similar results with the measurements of Foord *et al.*. The future study will be focused on the importance and the role of the neutral species in the early implosion phase.

ACKNOWLEDGMENTS

This work has been supported by the Basic Science Research Institute Program, Ministry of Education, 1995 (Project No. BSRI-95-2439) and the Korea Science and Engineering Foundation (Project No. 951-0205-017-2).

[1]P. G. Burkhalter, J. Shiloh, A. Fisher, and R. D. Cowan, J. Appl. Phys. **50**, 4532 (1979).
[2]N. R. Pereira and J. Davis, J. Appl. Phys. **64**, R1 (1988).
[3]I. N. Weinberg and A. Fisher, Nucl. Instrum. Methods Phys. Res. A **242**, 535 (1986).
[4]S. Maxon and T. Wainwright, Phys. Fluids **27**, 2535 (1984).
[5]G. Mehlman, P. G. Burkhalter, S. J. Stephanakis, F. C. Young, and D. J. Nagel, J. Appl. Phys. **60**, 3427 (1986).
[6]C. Deeney, P. D. LePell, F. L. Cochran, M. C. Coulter, K. G. Whitney, and J. Davis, Phys. Fluids B **5**, 992 (1993).
[7]W. Clark, R. Rechardson, J. Brannon, M. Wilkinson, and J. Katzenstein, J. Appl. Phys. **53**, 5552 (1982).
[8]C. R. Li and T. C. Yang, J. Phys. D **24**, 48 (1991).
[9]V. V. Vikhrev and S. I. Braginskii, *Reviews of Plasma Physics*, edited by M. A. Leontovich (Consultants Bureau, New York, 1986), Vol. 10, p. 425.
[10]M. E. Foord, Y. Maron, G. Davara, L. Gregorian, and A. Fisher, Phys. Rev. Lett. **72**, 3827 (1994).
[11]G. Barak and N. Rostoker, Appl. Phys. Lett. **41**, 918 (1982).
[12]K. T. Lee, S. H. Kim, D. Kim, and T. N. Lee, Phys. Plasmas **3**, 1340 (1996).
[13]R. L. Bowess and J. R. Wilson, *Numerical Modeling in Applied Physics and Astrophysics* (Jones and Bartlett, Boston, 1991), Chap. 4.
[14]D. Duchs and H. R. Griem, Phys. Fluids **9**, 1099 (1966).
[15]L. Spitzer, *Physics of Fully Ionized Gases*, 2nd ed. (Wiley, New York, 1962), Chap. 5.
[16]H. Fisser and J. Schlüter, Nucl. Fusion Suppl. Part 2, 571 (1962).
[17]J. Shiloh, ''High density Z-pinch,'' Ph.D. thesis, University of California, Irvine, 1978.